# Snake Robot Locomotion in Environments with Obstacles

Pål Liljebäck, *Member, IEEE,* Kristin Y. Pettersen, *Senior Member, IEEE,* Øyvind Stavdahl, *Member, IEEE,* and Jan Tommy Gravdahl, *Senior Member, IEEE*

***Abstract*—As a step towards enabling snake robots to move in cluttered environments, this paper proposes a control strategy that combines environment adaptation with directional control in order to achieve straight line path following control in environments with obstacles. Moreover, the paper presents the design of a mechanical snake robot with tactile sensing capabilities that allow the robot to sense its environment. Experimental results are presented where the snake robot is successfully propelled through different obstacle environments with the proposed control strategy.**

***Index Terms*—Underactuated Robots, Force and Tactile Sensing, Contact Modelling.**

## I. Introduction

INSPIRED by biological snake locomotion, snake robots carry the potential of meeting the growing need for robotic mobility in unknown and challenging environments. These mechanisms typically consist of serially connected joint modules capable of bending in one or more planes. The many degrees of freedom of snake robots make them difficult to control, but provide traversability in irregular environments that surpasses the mobility of the more conventional wheeled, tracked and legged forms of robotic mobility. A unique feature of snake robot locomotion compared to other forms of robotic mobility is that ground irregularities are beneficial for the propulsion since they provide push-points for the robot. The term *obstacle-aided locomotion* was introduced in [1] and captures the essence of this concept.

The majority of previous research on *control* of snake robots has focused on open-loop strategies for flat surface motion aimed at resembling gaits displayed by biological snakes (see e.g. [2]–[4]). Only a few works present control strategies related to obstacle-aided snake locomotion. Hirose [5] studied biological snakes and proposed a control strategy that used contact force sensing to *avoid* obstacles. In [6], an optimization problem is numerically solved in order to calculate the contact forces required to propel a snake robot in a desired direction. A kinematic approach is proposed in [7], where a curve fitting procedure is used to specify the body wave motion with respect to the obstacles. Environment adaptation of snake robots based solely on the measured joint angles and torques is considered in [8]–[10], while environment adaptation based on a measure of kinetic energy is considered in [11].

Manuscript received December 20, 2010.

Affiliation of Pål Liljebäck is shared between the Dept. of Engineering Cybernetics at the Norwegian University of Science and Technology (NTNU), NO-7491 Trondheim, Norway, and SINTEF ICT, Dept. of Applied Cybernetics, N-7465 Trondheim, Norway. E-mail: Pal.Liljeback@sintef.no.

Kristin Y. Pettersen, Øyvind Stavdahl, and Jan Tommy Gravdahl are with the Dept. of Engineering Cybernetics at the Norwegian University of Science and Technology (NTNU), NO-7491 Trondheim, Norway. E-mail: {Kristin.Y.Pettersen, Oyvind.Stavdahl, Tommy.Gravdahl}@itk.ntnu.no.

Enabling physical snake robots to sense their environment has received very limited focus in the literature so far. The wheeled snake robot developed by Hirose already in 1972 [5] was equipped with discrete contact switches. A snake robot with active wheels, where each wheel axis is equipped with a 3-axial force sensor, is presented in [12]. [7] presents a wheel-less snake robot with discrete contact switches. A snake robot with passive wheels equipped with strain gauge sensors is proposed in [13], while [14] presents a snake robot that uses force sensing resistors to detect and, to some extent, assess the magnitude of external forces.

This paper builds on previous work by the authors in [15], [16], where we investigate a control principle aimed at resolving situations where a snake robot is jammed between obstacles. The first contribution of this paper is a straight line path following controller for snake robots in obstacle environments. The main contribution of the controller is a strategy for continuously performing body shape adaptation to the environment in parallel with the cyclic body wave motion. The second contribution is the design of a mechanical snake robot with tactile sensing capabilities. The robot has a smooth surface in order to allow slithering (gliding) motion in cluttered environments, and is covered by contact force sensors to enable environment sensing. To our best knowledge, this is the first reported snake robot that can measure the magnitude of external forces applied along its body. Experimental results are presented where the physical snake robot is successfully propelled through different obstacle environments with the proposed control strategy.

Note that this paper only considers planar (2D) snake robot locomotion since we believe the essential control principles of snake robot locomotion are contained in a planar perspective. Moreover, we believe the simpler case of planar obstacle-aided locomotion should be fully understood before the more challenging problem of three-dimensional locomotion is considered.

This paper is based on and extends preliminary work by the authors in [17]–[19]. The extensions in this paper include the experimental results and general improvements of the overall presentation of the material.

The paper is organized as follows. Section II summarizes a mathematical model of a snake robot in an environment with obstacles. The path following controller and corresponding simulation results are presented in Sections III and IV, respectively. The design of the mechanical snake robot is presented in Section V, along with an experimental investigation of its contact force measurement system in Section VI. Section VII presents experimental results that illustrate the performance of the proposed controller. Finally, Section VIII presents concluding remarks.

## II. The Model of the Snake Robot

This section summarizes a model of the snake robot and introduces notation that will be employed to formulate the control strategy in Section III. A more detailed presentation of the model is presented in [15].

The snake robot is illustrated in Fig. 1(a) and consists of $N$ links of length $2l$, mass $m$, and moment of inertia $J$. The links are interconnected by $N-1$ joints and the actuator torque at joint $i \in \{1,\dots,N-1\}$ is denoted by $u_i$. The snake robot moves in the horizontal plane and has $N+2$ degrees of freedom. The position of the CM (center of mass) of the robot is denoted by $\boldsymbol{p} = (p_x, p_y)$ and the absolute angle $\theta_i$ of link $i \in \{1,\dots,N\}$ is expressed with respect to the global $x$ axis with counterclockwise positive direction. The angle of joint $i \in \{1,\dots,N-1\}$ is defined as

$$\phi_i = \theta_i - \theta_{i+1}, \tag{1}$$

and the joint angles are assembled in the vector $\boldsymbol{\phi} = [\phi_1,\dots,\phi_{N-1}]^T \in \mathbb{R}^{N-1}$. Moreover, we define the heading $\overline{\theta}$ of the robot as the average of the link angles, i.e. as

$$\overline{\theta} = \frac{1}{N}\sum_{i=1}^{N}\theta_i. \tag{2}$$

The heading-adjusted angle of link $i \in \{1,\dots,N\}$ is denoted by $\widetilde{\theta}_i$ and is given as the angle of link $i$ with respect to the current heading $\overline{\theta}$ (see Fig. 1(b)), i.e. as

$$\widetilde{\theta}_i = \theta_i - \overline{\theta}. \tag{3}$$

Furthermore, the forward velocity (tangential velocity) of the robot, denoted by $\overline{v}_t$, is defined as the component of the CM velocity $\dot{\boldsymbol{p}}$ along the current heading $\overline{\theta}$ (see Fig. 1(b)), i.e. as

$$\overline{v}_t = \dot{p}_x\cos\overline{\theta} + \dot{p}_y\sin\overline{\theta}. \tag{4}$$

The planar environment of the snake robot contains obstacles with circular shape. The interaction between a snake robot link and an obstacle is modelled by introducing a unilateral velocity constraint for the contacted link. The constraint is *unilateral* (acts in one lateral direction only) since the constraint shall allow sideways motion of the link *away* from the obstacle, but prevent any sideways motion *towards* (and thereby into) the obstacle (see [15] for details). The friction coefficient between the links and the obstacles is $\mu_o$, and the ground friction coefficient is $\mu$.

The measured contact force on link $i \in \{1,\dots,N\}$ is denoted by $\rho_i \in \mathbb{R}$ (see Fig. 1(b)) and we define $\boldsymbol{\rho} = [\rho_1,\dots,\rho_N]^T \in \mathbb{R}^N$. Moreover, the *propulsive component* of the measured force on link $i \in \{1,\dots,N\}$ is denoted by $\rho_{\mathrm{prop},i} \in \mathbb{R}$ and is given as the component of the normal direction contact force on the link along the current heading $\overline{\theta}$ (see Fig. 1(b)), i.e. as

$$\rho_{\mathrm{prop},i} = -\rho_i\sin\widetilde{\theta}_i. \tag{5}$$

The complete hybrid model of the snake robot is presented in [15] and will not be detailed here due to space restrictions.

## III. Straight Line Path Following Control in Obstacle Environments

In this section, we propose a straight line path following controller for snake robots in environments with obstacles.

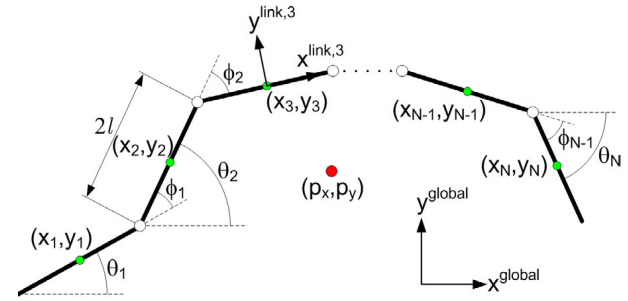


(a) The kinematic parameters of the snake robot.

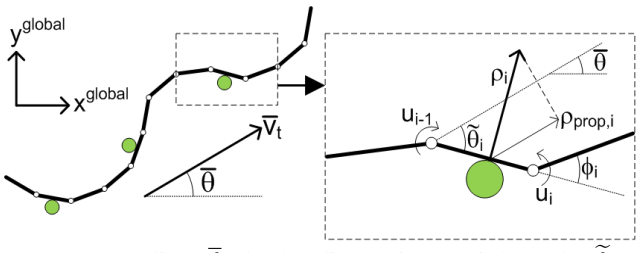


(b) The heading, $\overline{\theta}$, the heading-adjusted link angle, $\widetilde{\theta}_i$, and the propulsive contact force component, $\rho_{\mathrm{prop},i}$.

Fig. 1. Parameters of the snake robot.

### A. Control Objective

The control objective is to steer the snake robot so that it converges to and subsequently tracks a straight path while maintaining a heading which is parallel to the path. To this end, we define the global coordinate system so that the global $x$ axis is aligned with the desired straight path. The position of the snake robot along the global $y$ axis, $p_y$, is therefore the shortest distance from the robot to the desired path (i.e. the cross-track error) and the heading $\overline{\theta}$ of the robot is the angle that the robot forms with the desired path. The control objective is thereby to regulate $p_y$ and $\overline{\theta}$ so that they oscillate about zero while maintaining some nonzero forward velocity $\overline{v}_t > 0$. We will not attempt to make $p_y$ and $\overline{\theta}$ stay identical to zero since the heading and position of a snake robot will generally oscillate during locomotion.

### B. The Framework of the Path Following Controller

Snake robot locomotion is generally achieved by producing body waves that interact with the environment in order to push the robot forward [20]. Previous studies on obstacle-aided locomotion presented by the authors in [15], [16] suggest that this body wave motion should *not* be conducted in open-loop, but rather adjusted continuously according to the interaction of the robot with its environment. Furthermore, the motion must necessarily also be adjusted continuously in order to steer the robot in a desired direction. From the above discussion, we now propose a general framework for snake locomotion control where the joint reference angles $\boldsymbol{\phi}_{\mathrm{ref}} = [\phi_{1,\mathrm{ref}},\dots,\phi_{N-1,\mathrm{ref}}]^T \in \mathbb{R}^{N-1}$ are specified as the sum of three individual motion components, namely as

$$\boldsymbol{\phi}_{\mathrm{ref}} = \boldsymbol{\phi}_{\mathrm{wave}} + \boldsymbol{\phi}_{\mathrm{adapt}} + \boldsymbol{\phi}_{\mathrm{heading}}, \tag{6}$$

where $\boldsymbol{\phi}_{\mathrm{wave}}$ is a *body wave* component that induces propulsive forces on the robot from the environment, $\boldsymbol{\phi}_{\mathrm{adapt}}$ is an *environment adaptation* component that adjusts the body shape to the

environment, and $\boldsymbol{\phi}_{\text{heading}}$ is a *heading control* component. In the following subsections, we will propose a straight line path following controller for snake robots based on the controller framework defined in (6).

*Remark 1:* The *serpenoid curve* motion proposed by Hirose [5], which is considered in the majority of the snake robot literature, fits nicely within the framework proposed in (6). This gait pattern is achieved by controlling joint $i$ of the snake robot according to

$$\phi_{i,\text{ref}} = \underbrace{\alpha \sin\left(\omega t + (i-1)\,\delta\right)}_{\boldsymbol{\phi}_{\text{wave}}} + \underbrace{\phi_o}_{\boldsymbol{\phi}_{\text{heading}}}, \tag{7}$$

where the sinus term constitutes the body wave component, $\boldsymbol{\phi}_{\text{wave}}$, and $\phi_o$ is an angular offset which constitutes the heading component, $\boldsymbol{\phi}_{\text{heading}}$. The gait pattern does not involve environment adaptation, which means that $\boldsymbol{\phi}_{\text{adapt}} = \mathbf{0}$.

### C. The Body Wave Component

We employ a *predecessor-follower* scheme to specify the body wave component $\boldsymbol{\phi}_{\text{wave}}$, where each joint follows the angle of the preceding joint ahead of itself with a specified time delay $\Delta t$. The angle of joint $i$ is always a suitable reference angle for joint $i-1$ since the current shape of the snake robot always represents a feasible reference trajectory. The resulting reference angle of joint $i \in \{1, \ldots, N-2\}$ is therefore given as

$$\phi_{\text{wave},i}(t) = \phi_{i+1}(t - \Delta t). \tag{8}$$

In order to produce body wave motion, we introduce a sinusoidal reference angle for the heading-adjusted angle of the head link, $\widetilde{\theta}_N$, given by

$$\widetilde{\theta}_{N,\text{ref}}(t) = \alpha \sin(\omega t), \tag{9}$$

where $\alpha$ and $\omega$ are the amplitude and angular frequency, respectively, of the sinusoidal motion. Since it follows from (1) that $\phi_{N-1} = \widetilde{\theta}_{N-1} - \widetilde{\theta}_N$, we can track the head link reference angle in (9) by controlling the head joint according to the reference

$$\phi_{\text{wave},N-1}(t) = \widetilde{\theta}_{N-1} - \alpha \sin(\omega t). \tag{10}$$

From (8) and (10), we can now write the complete body wave component $\boldsymbol{\phi}_{\text{wave}}$ in matrix form as

$$\boldsymbol{\phi}_{\text{wave}} = \boldsymbol{S}_{\text{head}} \left(\widetilde{\theta}_{N-1} - \alpha \sin(\omega t)\right) + \boldsymbol{S}_{\text{joints}} \boldsymbol{\phi}(t - \Delta t), \tag{11}$$

where $\boldsymbol{\phi}(t - \Delta t)$ are the measured joint angles at time $t - \Delta t$, and where $\boldsymbol{S}_{\text{head}}$ and $\boldsymbol{S}_{\text{joints}}$ are, respectively, a selection vector and a selection matrix defined as

$$\boldsymbol{S}_{\text{head}} = [0, \ldots, 0, 1]^T \in \mathbb{R}^{N-1}, \tag{12}$$

$$\boldsymbol{S}_{\text{joints}} = \begin{bmatrix} 0 & 1 & 0 & & \\ & 0 & 1 & 0 & \\ & & \ddots & \ddots & \\ & & & 0 & 1 \\ & & & & 0 \end{bmatrix} \in \mathbb{R}^{(N-1)\times(N-1)}. \tag{13}$$

### D. The Environment Adaptation Component

We base the adaptation strategy on a control principle previously proposed in [15], where the links affected by contact forces are rotated so that the propulsive component of each contact force increases. Since the propulsive force components are what propel the snake robot forward, we conjecture that this approach will adapt the body shape to the environment in a way that maintains or increases the propulsion of the robot. The change of the propulsive force on link $i \in \{1, \ldots, N\}$ due to a change of the link angle is found by differentiating (5) with respect to $\widetilde{\theta}_i$, which gives

$$\frac{\partial \rho_{\text{prop},i}}{\partial \widetilde{\theta}_i} = -\rho_i \cos \widetilde{\theta}_i. \tag{14}$$

During adaptation, we choose to rotate links with a high propulsive force gradient with respect to the link angle, which suggests that link $i$ is rotated according to

$$\Delta\widetilde{\theta}_{i,\text{ref}} = k_\rho \frac{\partial \rho_{\text{prop},i}}{\partial \widetilde{\theta}_i} = -k_\rho \rho_i \cos \widetilde{\theta}_i, \tag{15}$$

where $k_\rho > 0$ is a controller gain. Furthermore, we choose that the contact force on link $i$ only should affect the angle of link $i$, so that $\Delta\widetilde{\theta}_{i-1,\text{ref}} = \Delta\widetilde{\theta}_{i+1,\text{ref}} = 0$. Since we have from (1) that $\phi_i = \widetilde{\theta}_i - \widetilde{\theta}_{i+1}$, we can write the desired change of $\phi_{i-1}$ and $\phi_i$ due to the contact force on link $i$ as

$$\Delta\phi_{i-1,\text{ref}} = \Delta\widetilde{\theta}_{i-1,\text{ref}} - \Delta\widetilde{\theta}_{i,\text{ref}} = k_\rho \rho_i \cos \widetilde{\theta}_i, \tag{16}$$

$$\Delta\phi_{i,\text{ref}} = \Delta\widetilde{\theta}_{i,\text{ref}} - \Delta\widetilde{\theta}_{i+1,\text{ref}} = -k_\rho \rho_i \cos \widetilde{\theta}_i. \tag{17}$$

By combining the desired change of $\phi_i$ due to the contact forces on the link at each side of the joint, we get

$$\phi_{\text{adapt},i} = -k_\rho \left(\rho_i \cos \widetilde{\theta}_i - \rho_{i+1} \cos \widetilde{\theta}_{i+1}\right). \tag{18}$$

The complete environment adaptation component $\boldsymbol{\phi}_{\text{adapt}}$ can be written in matrix form as

$$\boldsymbol{\phi}_{\text{adapt}} = -k_\rho \boldsymbol{D} \operatorname{diag}(\boldsymbol{\rho}) \cos \widetilde{\boldsymbol{\theta}}, \tag{19}$$

where $\operatorname{diag}(\cdot)$ produces a diagonal matrix with the elements of its argument along its diagonal, and where

$$\boldsymbol{\rho} = [\rho_1, \ldots, \rho_N]^T \in \mathbb{R}^N, \tag{20}$$

$$\cos \widetilde{\boldsymbol{\theta}} = \left[\cos \widetilde{\theta}_1, \ldots, \cos \widetilde{\theta}_N\right]^T \in \mathbb{R}^N, \tag{21}$$

$$\boldsymbol{D} = \begin{bmatrix} 1 & -1 & & & \\ & \ddots & \ddots & & \\ & & \ddots & \ddots & \\ & & & 1 & -1 \end{bmatrix} \in \mathbb{R}^{(N-1)\times N}. \tag{22}$$

### E. The Heading Control Component

The heading control component $\boldsymbol{\phi}_{\text{heading}}$ of the joint reference angles is similar to the guidance law employed in [20]–[22], where we considered straight line path following control of snake robots on flat surfaces without obstacles. In particular, we steer the snake robot towards the desired straight path by employing the Line-of-Sight (LOS) guidance law

$$\overline{\theta}_{\text{ref}} = -\arctan\left(\frac{p_y}{\Delta}\right), \tag{23}$$

where $p_y$ is the cross-track error and $\Delta > 0$ is a design parameter referred to as the *look-ahead distance* that influences

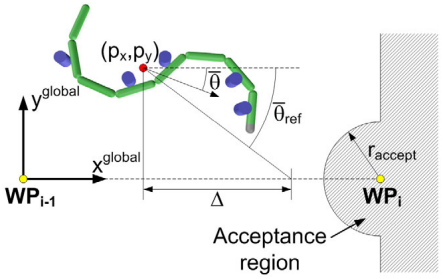


Fig. 2. Straight line path following control of the snake robot combined with waypoint guidance in an obstacle environment.

the rate of convergence to the desired path. As illustrated in Fig. 2, the LOS angle $\overline{\theta}_{\text{ref}}$ corresponds to the orientation of the snake robot when it is headed towards the point located a distance $\Delta$ ahead of itself along the desired path.

The locomotion direction of a snake robot is changed by introducing an offset in the joint reference angles (see e.g. [3], [23]). To steer the heading $\overline{\theta}$ according to the LOS angle in (23), we therefore offset the reference angle of the head joint according to

$$\phi_{\text{heading},N-1} = k_\theta \left(\overline{\theta} - \overline{\theta}_{\text{ref}}\right), \tag{24}$$

where $k_\theta > 0$ is a controller gain. Using (12), the heading component can be written in matrix form as

$$\boldsymbol{\phi}_{\text{heading}} = \boldsymbol{S}_{\text{head}} k_\theta \left(\overline{\theta} - \overline{\theta}_{\text{ref}}\right). \tag{25}$$

### F. The Joint Angle Controller

In order to make the joint angles $\boldsymbol{\phi} \in \mathbb{R}^{N-1}$ track the reference angles given by $\boldsymbol{\phi}_{\text{ref}} \in \mathbb{R}^{N-1}$, we set the joint actuator torques $\boldsymbol{u} \in \mathbb{R}^{N-1}$ according to the PD-controller

$$\boldsymbol{u} = k_p \left(\boldsymbol{\phi}_{\text{ref}} - \boldsymbol{\phi}\right) + k_d \left(\dot{\boldsymbol{\phi}}_{\text{ref}} - \dot{\boldsymbol{\phi}}\right), \tag{26}$$

where $k_p > 0$ and $k_d > 0$ are controller gains.

### G. Summary of the Path Following Controller

In accordance with the general controller framework defined in (6), we conjecture that the control objective stated in Section III-A is achieved by employing the PD-controller in (26) to control the joint angles of the snake robot according to

$$\boldsymbol{\phi}_{\text{ref}} = \boldsymbol{\phi}_{\text{wave}} + \boldsymbol{\phi}_{\text{adapt}} + \boldsymbol{\phi}_{\text{heading}}, \tag{27}$$

where

$$\boldsymbol{\phi}_{\text{wave}} = \boldsymbol{S}_{\text{head}} \left(\widetilde{\theta}_{N-1} - \alpha \sin(\omega t)\right) + \boldsymbol{S}_{\text{joints}} \boldsymbol{\phi}(t - \Delta t), \tag{28}$$

$$\boldsymbol{\phi}_{\text{adapt}} = -k_\rho \boldsymbol{D} \operatorname{diag}(\boldsymbol{\rho}) \cos \widetilde{\boldsymbol{\theta}}, \tag{29}$$

$$\boldsymbol{\phi}_{\text{heading}} = \boldsymbol{S}_{\text{head}} k_\theta \left(\overline{\theta} - \overline{\theta}_{\text{ref}}\right). \tag{30}$$

*Remark 2:* Due to the complexity of the hybrid model of the snake robot, we are currently unable to provide a formal proof of the achievement of the control objective stated in Section III-A with the proposed controller.

## IV. Simulation Study: The Performance of the Waypoint Guidance Strategy

This section presents simulation results that illustrate the performance of the proposed path following controller.

### A. Simulation Setup

The hybrid model of the snake robot and the path following controller were implemented in *Matlab R2008b*. The parameters of the snake robot were $N = 10$, $l = 0.07$ m, $m = 1$ kg, and $J = 0.0016$ kgm$^2$. Circular obstacles measuring 10 cm in diameter were placed in a random fashion in the environment of the snake robot. The ground and obstacle friction coefficients were $\mu = 0.3$ and $\mu_o = 0.25$, respectively. The initial link angles and position of the robot were $\boldsymbol{\theta} = [-30°, -10°, 30°, 60°, 40°, 0°, -40°, -60°, -30°, 0°]^T$ and $\boldsymbol{p} = \boldsymbol{0}$.

In order to study the path following controller from different initial conditions, we combined the controller with a simple waypoint guidance strategy previously proposed by the authors in [24]. The strategy is basically to interconnect waypoints by straight lines and perform path following along each straight line to control the robot to each waypoint. This approach is illustrated in Fig. 2, where $WP_i$ denotes the $i$th waypoint. The guidance strategy switches to the next waypoint as soon as the position of the robot enters inside the *acceptance region* of the current waypoint, which is illustrated in Fig. 2. The reader is referred to [24] for more details about this guidance strategy.

We defined five waypoints with global frame coordinates $(2.5, 0)$, $(2.5, 1)$, $(0, 1)$, $(1, 2)$, and $(3, 2)$, respectively, and with acceptance circle radius $r_{\text{accept}} = 0.5$ m. The controller parameters were $\Delta = 0.7$ m, $k_\theta = 1.3$, $k_\rho = 0.02$, $\Delta t = 0.7$ s, $\alpha = 60°$, $\omega = 40°$/s, $k_p = 20$, and $k_d = 5$. Furthermore, we low-pass filtered $\boldsymbol{\phi}_{\text{ref}}$ at 0.75 Hz to prevent steps in $\boldsymbol{\phi}_{\text{ref}}$ due to the measured contact forces in $\boldsymbol{\phi}_{\text{adapt}}$.

### B. Simulation Results

The simulation result is shown in Fig. 3 and Fig. 4. In particular, the path of the centre link of the snake robot (link 5) is shown in blue in Fig. 3, where black squares indicate the waypoints, the dotted black lines indicate the straight paths between the waypoints, and where the shape and position of the robot are shown in green at $t = 0$ s, $t = 65$ s, and $t = 125$ s, respectively. Furthermore, Fig. 4 shows the cross-track error $p_y$, the heading angle $\overline{\theta}$, the forward velocity $\overline{v}_t$, and the obstacle constraint force on the centre link, where vertical dashed lines indicate time instants where the guidance strategy switched to the next waypoint. Fig. 3 shows that the propulsion of the robot was maintained through all the waypoints. Furthermore, Fig. 4 shows that the forward velocity varied between 5 - 10 cm/s, and that the cross-track error and heading angle had an oscillatory behaviour near zero before each waypoint switch. The simulation result therefore suggests that the control objective stated in Section III-A was achieved.

## V. Development of a Mechanical Snake Robot for Obstacle-Aided Locomotion

This section presents the design of a snake robot with tactile sensing capabilities. To our best knowledge, this is the first reported snake robot that can measure the magnitude of external forces applied along its body. We will use this snake robot in Section VII to experimentally investigate the controller from Section III.

### A. Overview of the Snake Robot Design

Intelligent and efficient snake robot locomotion requires that the snake robot can *sense* its environment, which can be

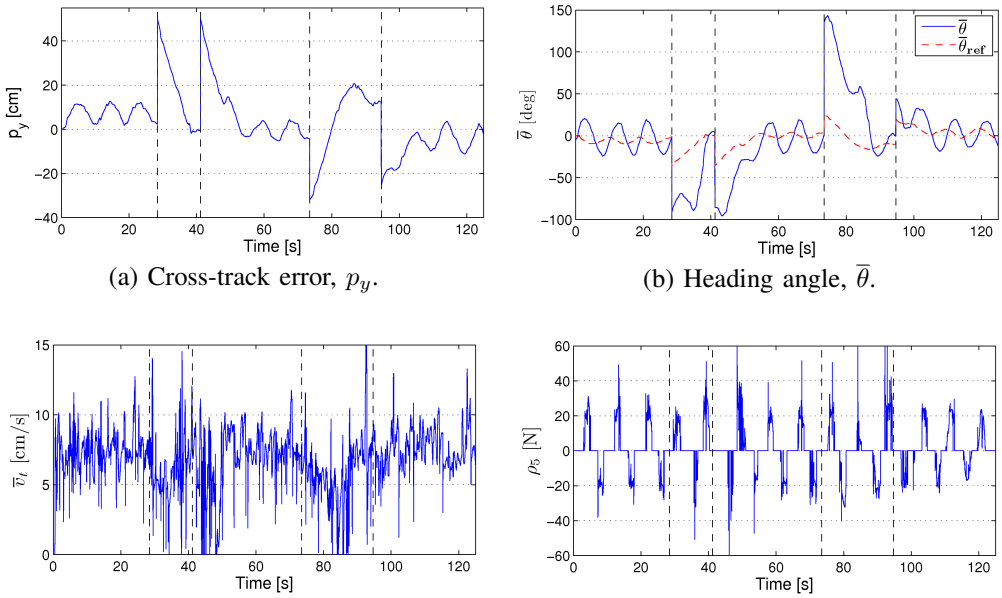


(a) Cross-track error, $p_y$. (b) Heading angle, $\overline{\theta}$.

(c) Forward velocity, $\overline{v}_t$. (d) Obstacle constraint force on link 5, $\rho_5$.

Fig. 4. State trajectories of the snake robot during path following between waypoints in an obstacle environment.

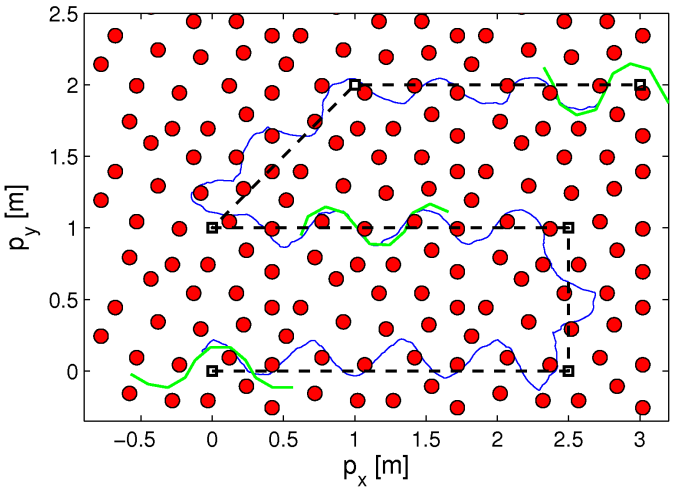


Fig. 3. The simulated path of the centre link (link 5) of the snake robot during path following between waypoints in an obstacle environment.

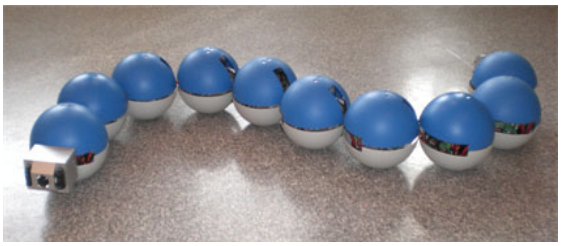

Fig. 5. The snake robot, *Kulko*.

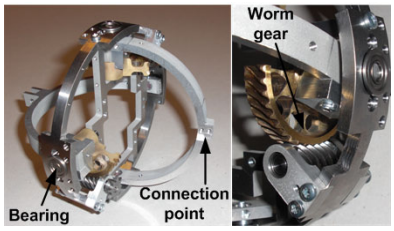


Fig. 6. The articulation mechanism of the joint modules.

achieved by equipping the robot with contact force sensing capabilities along its body. Furthermore, enabling a snake robot to glide forward in a cluttered environment requires that the body of the robot is sufficiently smooth, i.e. free of obstructive features. The snake robot described in the following, which we call *Kulko*, was developed to comply with both these requirements. In particular, the idea behind the robot is to encapsulate each joint module by a spherical shell that gives the joint a smooth outer surface independently of how the joint is flexed. Contact force sensing is thereby achieved by mounting force sensors underneath each spherical shell. As shown in Fig. 5, the complete snake robot consists of a serial connection of 10 identical ball-shaped joint modules. The smooth exterior surface and the force sensing capabilities of the robot are maintained independently of how the joints are flexed.

### B. The Joint Actuation Mechanism

The articulation mechanism of each joint module (see Fig. 6) has two degrees of freedom (pitch and yaw) and consists of two links supported by bearings in a steel ring. Each link has a connection point that allows it to be connected to the next joint module by two screws. The angle of the two moving links in the joint are measured with magnetic rotary encoders (AS5043 from austriamicrosystems). A magnet measuring 6 mm in diameter is attached to each link so that it rotates above the rotary encoder as shown in Fig. 7.

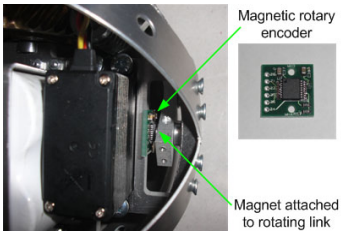


Fig. 7. Magnetic rotary encoder used for measuring the joint angle.

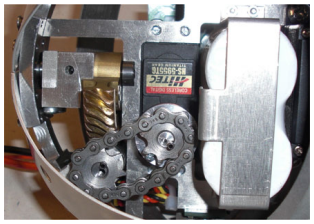

Fig. 8. Roller chain connecting the servo motor to the worm gear.

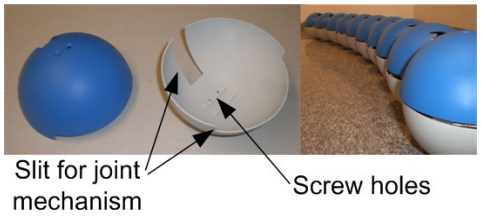


Fig. 9. Left: The upper and lower hemispherical shell of a joint module. Right: The smooth gliding surface along the snake robot.

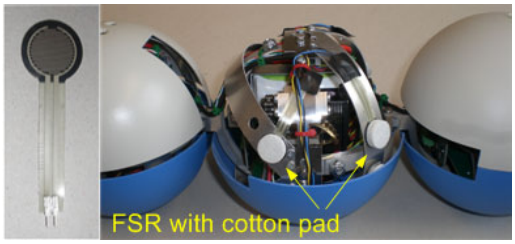


Fig. 10. Left: FSR (force sensing resistor) used to measure contact forces. Right: FSRs covered by cotton pads mounted to a joint module.

Each link is driven by a Hitec servo motor (HS-5955TG) by connecting the output shaft of each motor to a worm gear (gear ratio of 1:5.71) through a steel roller chain. The worm gear and the chain drive are shown in Fig. 6 and Fig. 8, respectively. Worm gears are mechanically robust and may essentially produce any desired gear ratio in a single gear stage, which facilitates a compact design. Table I lists the parameters characterizing the actuation mechanism.

### C. The Exterior Gliding Surface

The smooth exterior gliding surface of Kulko is obtained by covering each joint module by two hemispherical shells, as shown in Fig. 9. The shells, which were moulded from a plastic material, are 1.5 mm thick, weigh 42 g each, and have an outer diameter of 140 mm. Each shell is attached to the joint mechanism by two screws. The splice between the two hemispherical shells lies in the horizontal plane. The shells have a slit on each side corresponding to the range of motion of the connection points to the two neighbouring joints.

### D. The Contact Force Measurement System

*1) Assumptions Underlying the Sensor System:* Kulko was primarily developed to study obstacle-aided locomotion on horizontal surfaces with vertical obstacles, which corresponds to the environment captured by the hybrid model described in Section II. As a result, the contact force sensor system was implemented to primarily measure *horizontal* contact forces, although the design can be modified to measure contact forces of arbitrary direction. The sensor system measures contact forces with respect to the *macroscopic* shape of the snake robot. Information about the specific location of an applied force on the surface of a single joint module is not believed to be of significant interest. This means that the sensor system determines the *magnitude* of a contact force and also at which *side* of a joint module the force is applied. Furthermore, we assume that the direction of a contact force is *normal* to the macroscopic shape of the snake robot at the location where the force is applied. This approach is in line with the contact modelling approach of the hybrid model presented in Section II.

*2) The Sensor System Setup:* Four force sensing resistors (FSRs) with diameter 13 mm are mounted on each side of a joint module to measure contact forces. A FSR is a polymer thick film device that exhibits a decrease in electrical resistance when the force applied to the sensor increases. As shown to the right of Fig. 10, a small cotton pad (3 mm thick) is placed over each FSR in order to distribute the applied force across the entire sensor area. FSRs are not suited for precision measurements, but we conjecture that precise force measurements are not required during snake robot locomotion.

*3) Calculation of Contact Forces:* There is a near linear relationship between the force $F_{\text{FSR}}$ applied to the sensor area of a FSR and the inverse of the resulting electrical resistance $R_{\text{FSR}}$ through the sensor. By applying different known forces to a FSR and measuring the resulting electrical resistance, we were able to estimate that

$$F_{\text{FSR}} = \frac{18.9}{R_{\text{FSR}}}. \tag{31}$$

As explained in Section V-D2, each side of the joint mechanism is equipped with four FSRs. Since the shells are only in contact with the internal structure of the robot through the FSR measuring points, we estimate the magnitude of an external contact force by simply summing the forces measured at each FSR. Furthermore, any force measured when the robot is powered up, i.e. when there are no external forces acting on

TABLE I
PARAMETERS OF A JOINT MODULE.

| Parameter | Value |
|---|---|
| Total weight of a joint module | 960 g |
| Outer diameter | 130 mm |
| Degrees of freedom | 2 |
| Max joint travel | $\pm 45^\circ$ |
| Max continuous joint torque | 4.5 Nm |
| Max joint speed (no load) | $70^\circ/_{\text{sec}}$ |

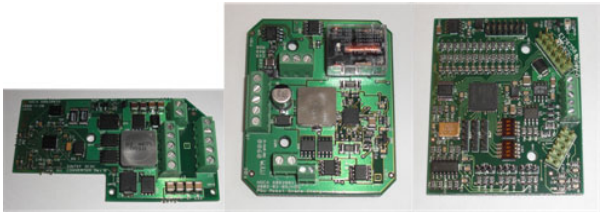

Fig. 11. Left: The voltage regulation card. Middle: The battery charger card. Right: The joint controller card.

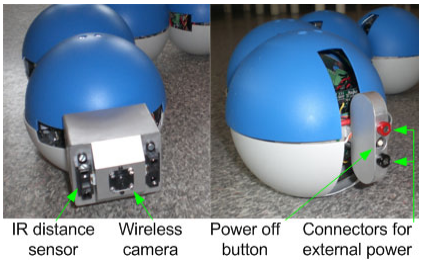


Fig. 12. Left: The head of the robot. Right: The tail of the robot.

the shells, represents an offset which is subtracted from the force measurements.

### E. The Power and Control System

Three custom-designed circuit boards, shown in Fig. 11, are installed in each joint module to handle power supply and motion control tasks. Each joint is powered by two serially connected Lithium Ion batteries (6.6V at about 2.3Ah), which are charged by a battery charger card (see the middle of Fig. 11). The charging is automatically initiated by applying an external voltage to the power connectors located at the tail of the snake robot (see the right of Fig. 12). Regulation of the voltage to the internal components of a joint is handled by the card shown to the left of Fig. 11.

Each joint module is controlled by the microcontroller card shown to the right of Fig. 11, which is based on the Atmel microcontroller AT90CAN128. This card continuously measures the joint angles and the contact forces, and generates PWM pulses for the servo motors (see Fig. 13). The card has a CAN bus interface for communicating with the other modules of the robot.

The brain (or head) of the snake robot, which is shown to the left of Fig. 12, contains the same microcontroller card that controls the motion of the joints. The brain card receives joint

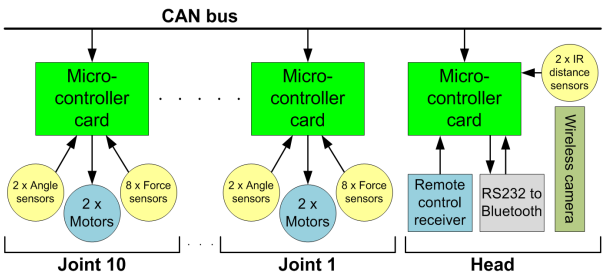


Fig. 13. The data flow between the modules of the snake robot.

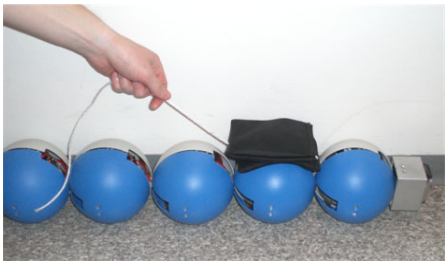

Fig. 14. The experimental investigation of the sensor system.

reference angles at about 20 Hz from an external computer via a wireless connection based on Bluetooth, and distributes the reference angles to the corresponding joint modules over the CAN bus. The head is also equipped with a small wireless camera and two IR distance sensors (see the left in Fig. 12).

## VI. Experimental Study: The Performance of the Contact Force Measurement System

The contact force measurement system of the snake robot was experimentally investigated as shown in Fig. 14. With the left side of the robot facing upwards, three different loads weighing 1350 g, 2750 g, and 4300 g, respectively, were dragged backwards along the robot. The resulting force measurements at joint 4, 5, and 6 (joint 1 is the head) are shown in Fig. 15. Despite some deviations, the measured forces agree fairly well with the weight of the loads. Note that the force plots have a triangular shape rather than the ideal rectangular shape, which suggests that the sensor system does not measure forces *between* the joints very well. However, we do not consider this to be a critical issue in order to demonstrate obstacle-aided locomotion, especially not if the obstacles are large compared to the size of each joint module.

## VII. Experimental Study: The Performance of the Environment Adaptation Strategy

In this section, we employ the snake robot Kulko to experimentally investigate the controller proposed in Section III.

### A. Experimental Setup

As shown in Fig. 16, the experiments were carried out on a horizontal surface with circular obstacles placed around the snake robot. The location of each obstacle could easily be changed by means of a grid of mounting holes in the floor. The horizontal position of the robot was measured at 15 Hz by use of three firewire cameras (Unibrain Fire-i 520c) mounted in the ceiling above the robot. The camera tracking software *SwisTrack* [25] was used to extract the position of three black circular markers (40 mm in diameter) mounted on the snake robot. SwisTrack estimated the maximum and the average position error to be about 1.9 cm and 0.6 cm, respectively. The global $x$ axis was configured to be parallel to the long side of the course. The CM position, $\boldsymbol{p}$, and the absolute link angles, $\boldsymbol{\theta}$, were calculated from the camera marker positions using simple kinematic relationships presented in [20].

The joint reference angles defined by (27) were calculated with the parameters $N = 10$, $l = 0.07$ m, $k_\rho = 0.01$, $\Delta t = 0.9$ s, $\alpha = 60°$, and $\omega = 30°$/s. Due to the limited range of the obstacle course, we did not consider heading

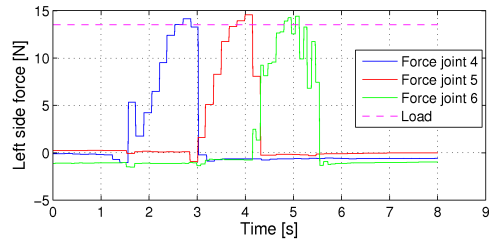


(a) Experiment with load weighing 1350 g.

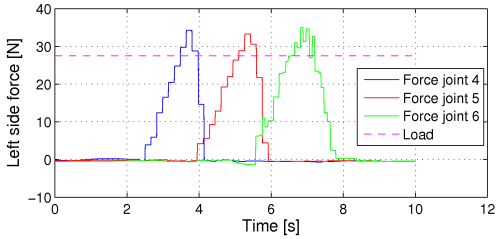


(b) Experiment with load weighing 2750 g.

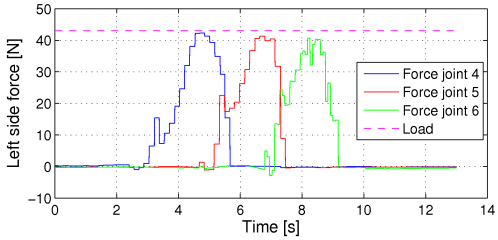


(c) Experiment with load weighing 4300 g.

Fig. 15. Forces measured by joints 4 - 6 when three different loads were dragged along the snake robot.

control during the experiments, which means that $\phi_{\text{heading}} = 0$. Moreover, the joint angles were not controlled according to (26), but instead according to the proportional controller of the servo motors used in the robot.

We considered three obstacle environments. The first obstacle environment contained five obstacles with $x$ coordinates $(-123.9, -89.6, -48.4, -8.2, -0.6)$ cm, $y$ coordinates $(20.2, -15.7, 13.2, -23.5, 24.8)$ cm, and diameters $(30, 20, 30, 30, 20)$ cm, respectively. The second obstacle environment contained four obstacles with $x$ coordinates $(-90.9, -35.5, 5.1, 31.7)$ cm, $y$ coordinates $(-20.3, 4.2, -28.9, 15.9)$ cm, and diameters $(30, 30, 30, 30)$ cm, respectively. The third and final obstacle environment contained five obstacles with $x$ coordinates $(-93.1, -79.4, -45.4, -17.4, 14.6)$ cm, $y$ coordinates $(-61.7, -6.3, 29.4, -18.9, 24.3)$ cm, and diameters $(30, 30, 20, 30, 30)$ cm, respectively. For all three environments, the initial position of the head link was $(x_N = 0, y_N = 0)$ and the initial link angles are visualized together with the experimental results.

### B. Experimental Results

The motion in the three obstacle environments are shown in Figures 17 and 18, Figures 19 and 20, and Figures 21 and 22, respectively. As seen from Figures 17(a), 19(a), and 21(a), the overall forward propulsion of the robot was maintained throughout all three trials, which was the main goal of the

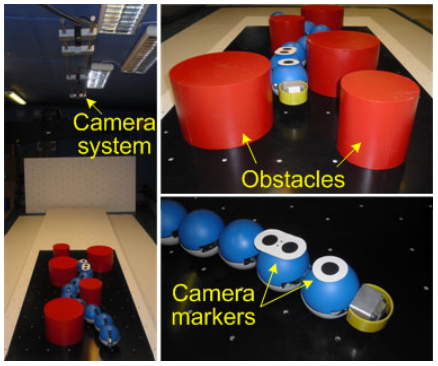


Fig. 16. The experimental setup. Three cameras mounted in the ceiling measured the position of the snake robot in a course with obstacles.

experiments. In other words, using the same controller with the same set of controller parameters, the snake robot was able to move through three different obstacle environments, which we consider to be evidence that the proposed control strategy provides a snake robot with environment adaptation skills.

The relatively slow forward speed of the robot was mainly due to the limited torque of the joints compared to the rather large ground and obstacle friction forces opposing the motion. In particular, the snake robot is rather heavy (about 10 kg) compared to its maximum actuator torque (about 4 Nm). To give an idea of the forces needed to propel the robot forward in the three environments, the measured contact forces on joint modules 4, 5, and 6 (counting module 1 as the tail) are shown in Figures 17(d), 19(d), and 21(d), respectively.

The measured (solid line) and the reference angles (dashed line) of joints 4 and 5 during the three trials are shown in Figures 17(e)-(f), 19(e)-(f), and 21(e)-(f), respectively. In accordance with (29), the measured contact forces on modules 4, 5, and 6 affect the reference angles of joints 4 and 5. To illustrate this effect, we have plotted the environment adaptation components of the reference angles, i.e. $\phi_{\text{adapt},4}$ and $\phi_{\text{adapt},5}$, with a dotted line together with the reference angles. It was clearly observed during the experiments that the adaptation component of the joint reference angles serves as a 'curvature generator' by producing more body curvature at locations where the robot makes contact with an obstacle. This curvature is subsequently propagated backwards by the body wave component in (28), which generates a push against the contacted obstacle.

In summary, the experimental results illustrate that a snake robot is propelled forward in an obstacle environment when the joints are controlled according to (27).

## VIII. Conclusions

This paper has proposed a straight line path following controller for snake robots in environments with obstacles. The main contribution of the controller is the strategy for continuously performing body shape adaptation to the environment. The paper has also presented the design of the snake robot *Kulko*, which combines a smooth outer surface (independently of how the joints are flexed) with contact force sensing capabilities. The function of the contact force measurement system was validated through experiments. Moreover, the paper has presented experimental results where the proposed

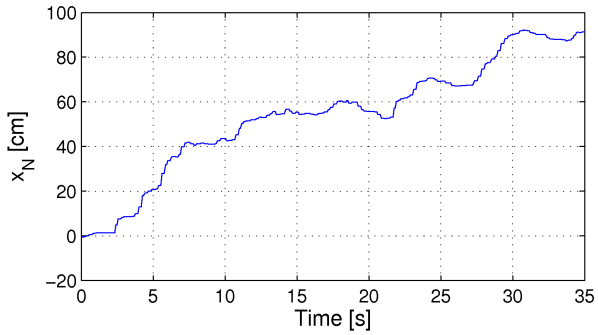


(a) The $x$ coordinate of the head.

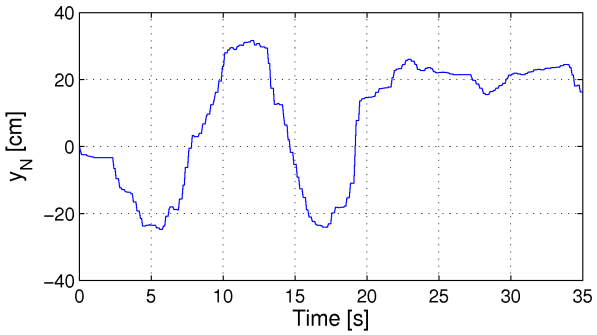


(b) The $y$ coordinate of the head.

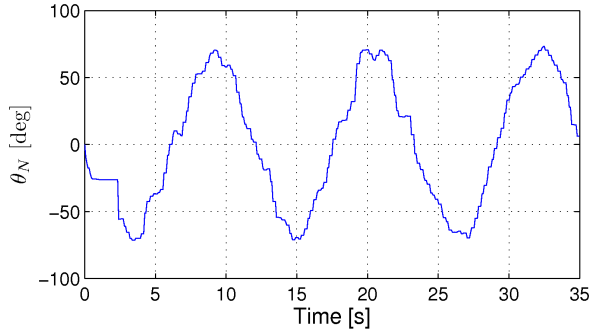


(c) The angle of the head link.

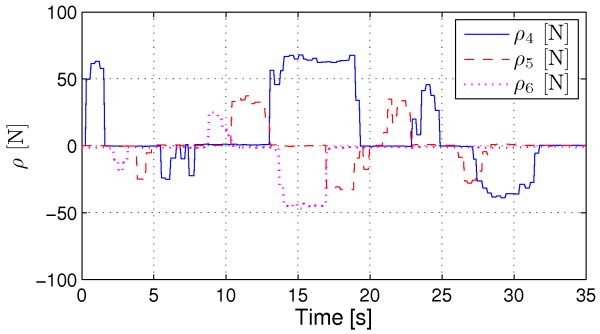


(d) Contact forces.

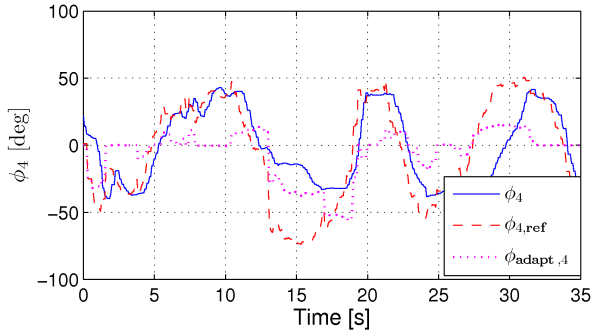


(e) The angle of joint 4.

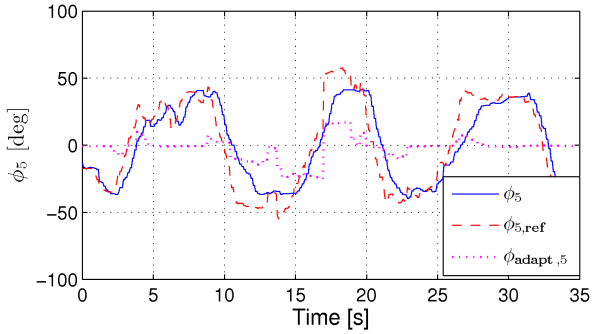


(f) The angle of joint 5.

Fig. 17. Experimental results of obstacle-aided locomotion in the first obstacle environment.

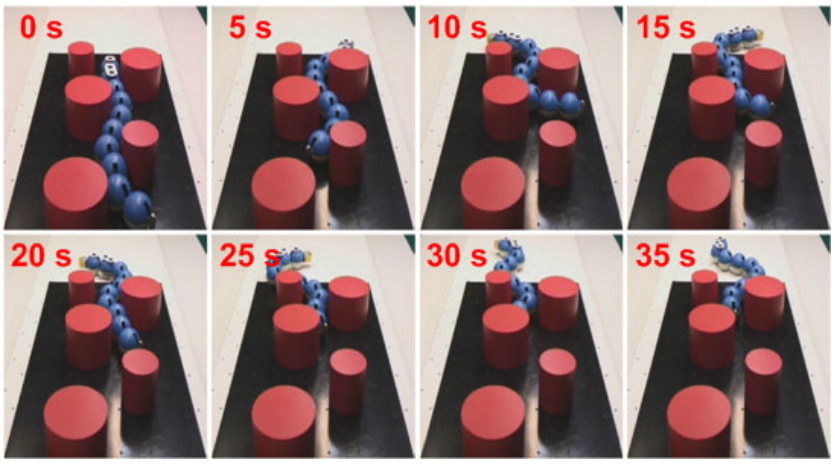


Fig. 18. The motion of the snake robot in the first obstacle environment.

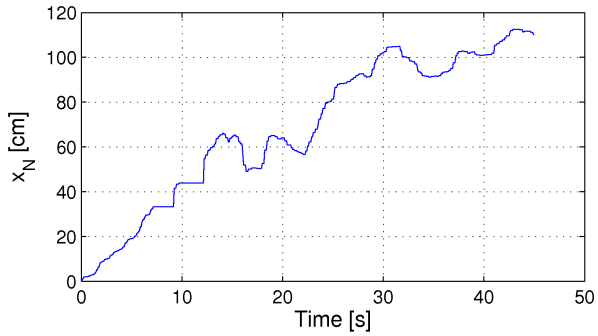


(a) The $x$ coordinate of the head.

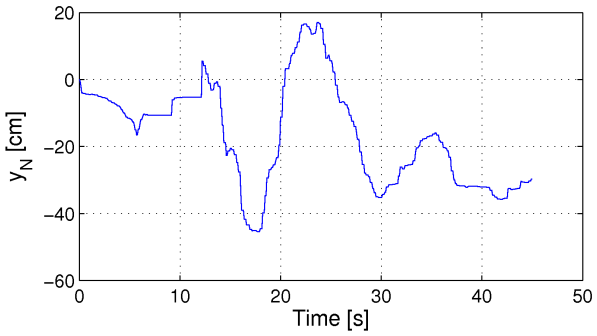


(b) The $y$ coordinate of the head.

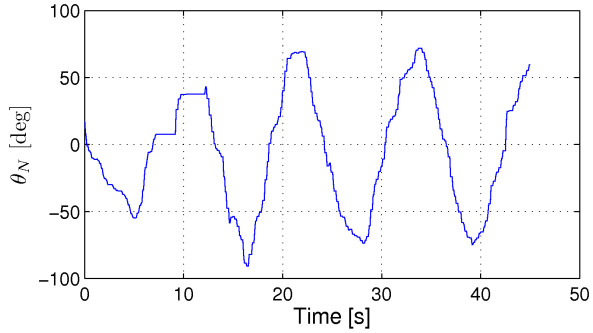


(c) The angle of the head link.

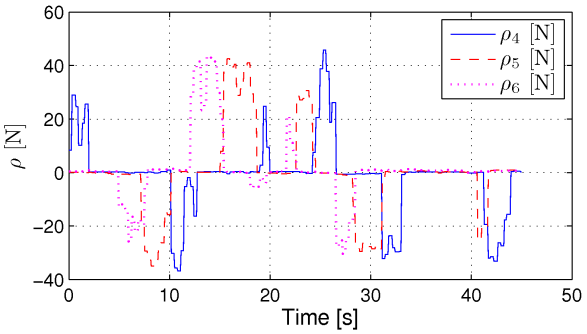


(d) Contact forces.

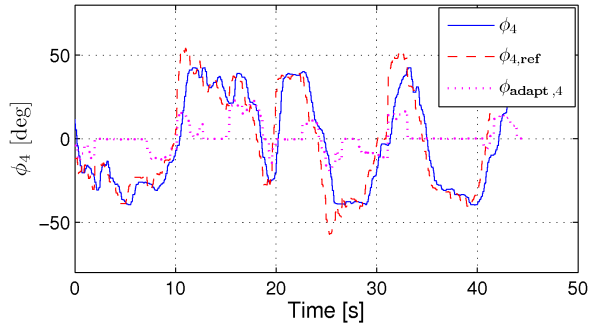


(e) The angle of joint 4.

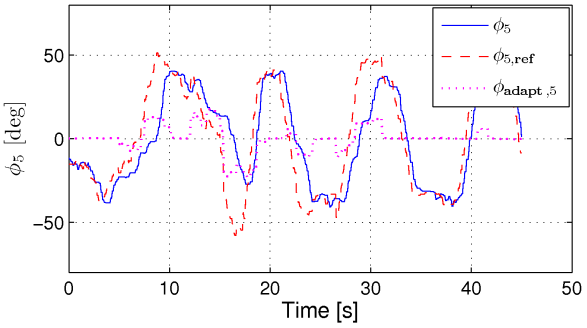


(f) The angle of joint 5.

Fig. 19. Experimental results of obstacle-aided locomotion in the second obstacle environment.

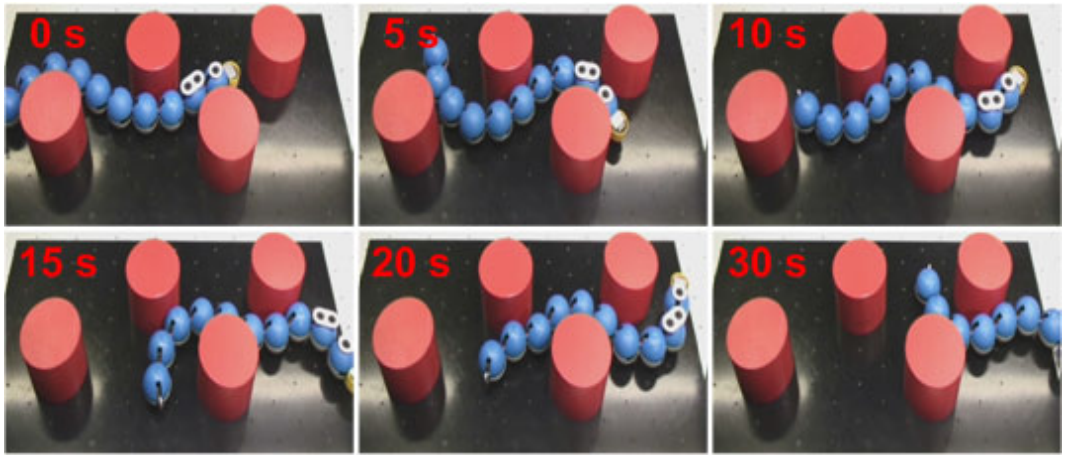


Fig. 20. The motion of the snake robot in the second obstacle environment.

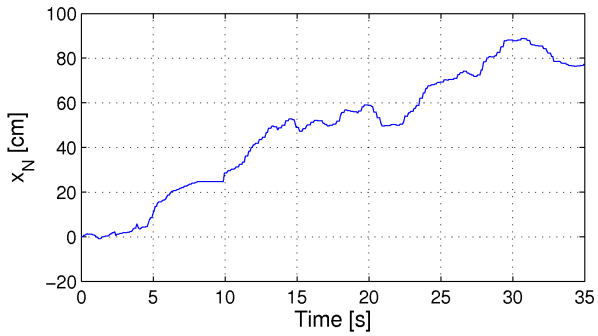


(a) The $x$ coordinate of the head.

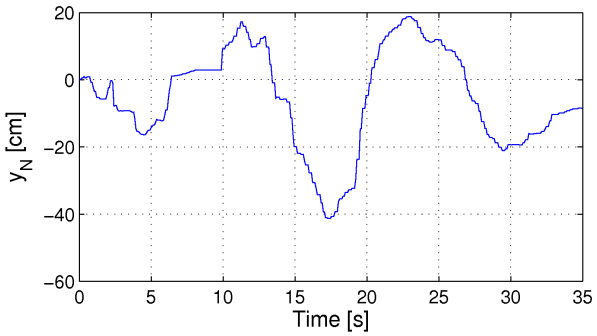


(b) The $y$ coordinate of the head.

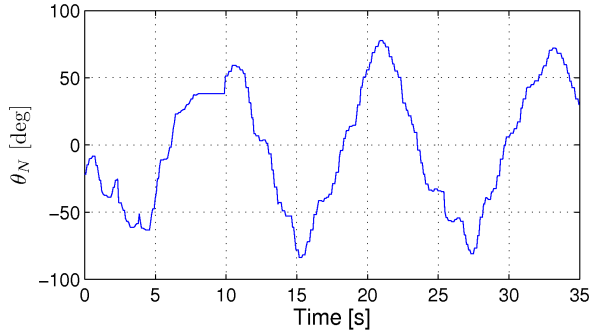


(c) The angle of the head link.

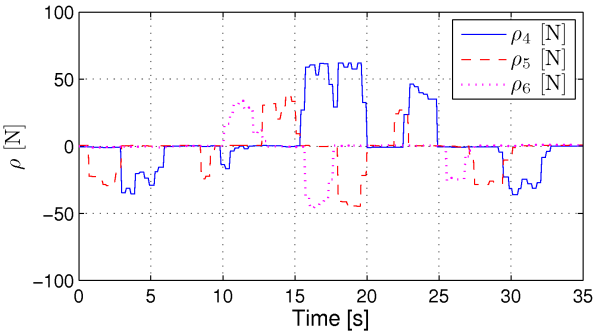


(d) Contact forces.

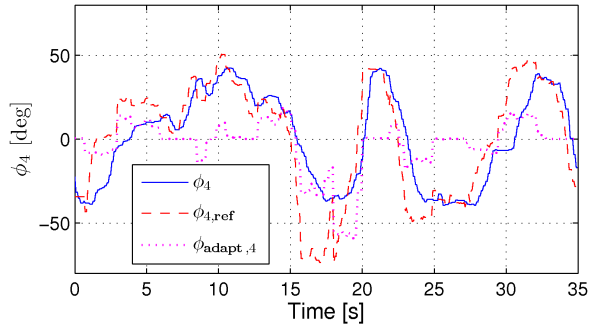


(e) The angle of joint 4.

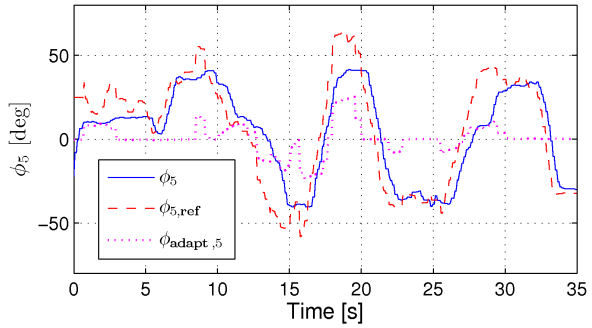


(f) The angle of joint 5.

Fig. 21. Experimental results of obstacle-aided locomotion in the third obstacle environment.

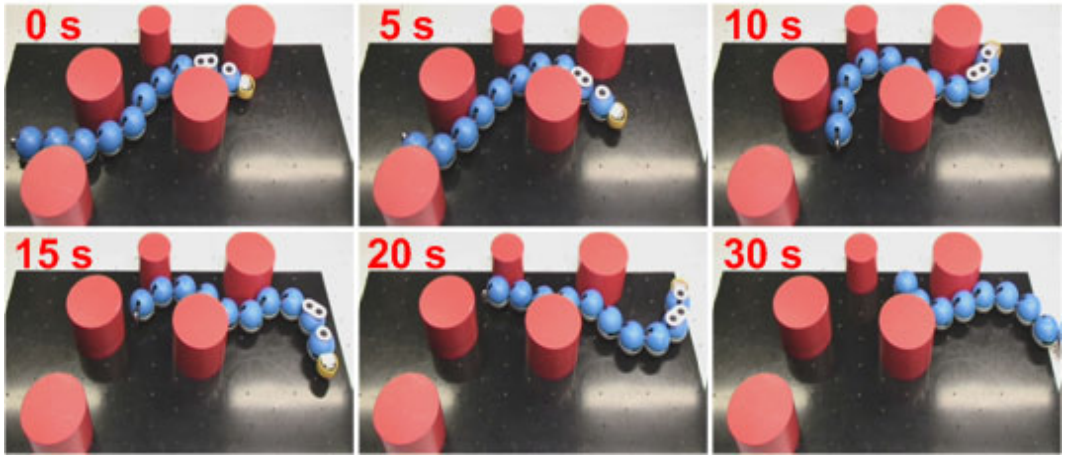


Fig. 22. The motion of the snake robot in the third obstacle environment.

controller successfully propelled the physical snake robot through different obstacle environments.

## REFERENCES


[1] A. A. Transeth, R. I. Leine, C. Glocker, K. Y. Pettersen, and P. Liljebäck, "Snake robot obstacle aided locomotion: Modeling, simulations, and experiments," *IEEE Trans. Rob.*, vol. 24, no. 1, pp. 88–104, 2008.

[2] S. Ma, "Analysis of creeping locomotion of a snake-like robot," *Adv. Robotics*, vol. 15, no. 2, pp. 205–224, 2001.

[3] M. Saito, M. Fukaya, and T. Iwasaki, "Serpentine locomotion with robotic snakes," *IEEE Contr. Syst. Mag.*, vol. 22, no. 1, pp. 64–81, February 2002.

[4] F. Chernousko, "Modelling of snake-like locomotion," *Appl. Math. Comput.*, vol. 164, no. 2, pp. 415–434, May 2005.

[5] S. Hirose, *Biologically Inspired Robots: Snake-Like Locomotors and Manipulators*. Oxford: Oxford University Press, 1993.

[6] Z. Bayraktaroglu and P. Blazevic, "Understanding snakelike locomotion through a novel push-point approach," *J. Dyn. Syst. - Trans. ASME*, vol. 127, no. 1, pp. 146–152, March 2005.

[7] Z. Y. Bayraktaroglu, "Snake-like locomotion: Experimentations with a biologically inspired wheel-less snake robot," *Mechanism and Machine Theory*, vol. 44, no. 3, pp. 591–602, 2008.

[8] H. Date and Y. Takita, "Adaptive locomotion of a snake like robot based on curvature derivatives," in *Proc. IEEE/RSJ Int. Conf. Intelligent Robots and Systems*, San Diego, CA, USA, Oct-Nov 2007, pp. 3554–3559.

[9] A. M. Andruska and K. S. Peterson, "Control of a snake-like robot in an elastically deformable channel," *IEEE/ASME Trans. Mechatronics*, vol. 13, no. 2, pp. 219–227, april 2008.

[10] A. Kuwada, S. Wakimoto, K. Suzumori, and Y. Adomi, "Automatic pipe negotiation control for snake-like robot," in *Proc. IEEE/ASME Int. Conf. on Advanced Intelligent Mechatronics*, July 2008, pp. 558–563.

[11] Z. Wang, S. Ma, B. Li, and Y. Wang, "Stability and adaptability of passive creeping of a snake-like robot," in *Proc. IEEE/RSJ Int. Conf. Intelligent Robots and Systems*, 2010, pp. 395–400.

[12] S. R. Taal, H. Yamada, and S. Hirose, "3 axial force sensor for a semi-autonomous snake robot," in *Proc. IEEE Int. Conf. Robotics and Automation*, 2009, pp. 4057–4062.

[13] T. L. T. Chen, S. Liu, and J. Yen, "A bio-mimetic snake-like robot: Sensor based gait control," in *Advanced robotics and Its Social Impacts, 2008. ARSO 2008. IEEE Workshop on*, 2008, pp. 1–6.

[14] S. A. Fjerdingen, J. R. Mathiassen, H. Schumann-Olsen, and E. Kyrkjeb, "Adaptive snake robot locomotion: A benchmarking facility for experiments," in *European Rob. Symp. 2008*, vol. 44, 2008, pp. 13 – 22.

[15] P. Liljebäck, K. Y. Pettersen, Ø. Stavdahl, and J. T. Gravdahl, "Hybrid modelling and control of obstacle-aided snake robot locomotion," *IEEE Trans. Robotics*, vol. 26, no. 5, pp. 781–799, Oct 2010.

[16] ——, "Experimental investigation of obstacle-aided locomotion with a snake robot," *IEEE Trans. Robotics*, 2011, to appear.

[17] P. Liljebäck, S. Fjerdingen, K. Y. Pettersen, and Ø. Stavdahl, "A snake robot joint mechanism with a contact force measurement system," in *Proc. IEEE Int. Conf. Robotics and Automation*, Kobe, Japan, 2009, pp. 3815–3820.

[18] P. Liljebäck, K. Y. Pettersen, and Ø. Stavdahl, "A snake robot with a contact force measurement system for obstacle-aided locomotion," in *Proc. IEEE Int. Conf. Robotics and Automation*, Anchorage, AK, USA, 2010, pp. 683–690.

[19] P. Liljebäck, K. Y. Pettersen, Ø. Stavdahl, and J. T. Gravdahl, "Path following control of snake robots in unstructured environments," in *Proc. IEEE Int. Conf. Robotics and Automation*, Shanghai, China, 2011.

[20] ——, "Controllability and stability analysis of planar snake robot locomotion," *IEEE Trans. Automatic Control*, vol. 56, no. 6, pp. 1365–1380, 2011.

[21] P. Liljebäck, I. U. Haugstuen, and K. Y. Pettersen, "Path following control of planar snake robots using a cascaded approach," in *Proc. IEEE Conf. Decision and Control*, Atlanta, GA, USA, 2010, pp. 1969–1976.

[22] ——, "Experimental investigation of a path following controller for planar snake robots," in *Proc. IEEE Int. Conf. Control, Automation, Robotics, and Vision (ICARCV)*, Singapore, 2010, pp. 2325–2332.

[23] P. Liljebäck, K. Y. Pettersen, Ø. Stavdahl, and J. T. Gravdahl, "A simplified model of planar snake robot locomotion," in *Proc. IEEE/RSJ Int. Conf. Intelligent Robots and Systems*, Taipei, Taiwan, 2010, pp. 2868–2875.

[24] P. Liljebäck and K. Y. Pettersen, "Waypoint guidance control of snake robots," in *Proc. IEEE Int. Conf. Robotics and Automation*, Shanghai, China, 2011.

[25] T. Lochmatter, P. Roduit, C. Cianci, N. Correll, J. Jacot, and A. Martinoli, "Swistrack - a flexible open source tracking software for multi-agent systems," in *IEEE/RSJ Int. Conf. Intelligent Robots and Systems*, 2008, pp. 4004–4010.


**Pål Liljebäck** (M'08) received his MSc and PhD degree in Electrical Engineering at the Norwegian University of Science and Technology (NTNU), Trondheim, Norway, in 2004 and 2011, respectively. He is currently a Post Doctoral researcher at the Department of Engineering Cybernetics, NTNU, and simultaneously works as a research scientist at SINTEF ICT, Department of Applied Cybernetics, Trondheim, Norway, which is a Norwegian research organization. His research interests include modelling and control of dynamical systems, and design and implementation of mechatronic systems.

**Kristin Y. Pettersen** (S'93–M'98–SM'04) received her MSc and PhD degree in Electrical Engineering at the Norwegian University of Science and Technology (NTNU), Trondheim, Norway, in 1992 and 1996 respectively. In 1996 she became Associate Professor, and in 2002 Professor, at the Department of Engineering Cybernetics, NTNU. In 1999 she was a Visiting Fellow at the Department of Mechanical and Aerospace Engineering, Princeton University, Princeton, NJ and in 2008 Visiting Professor at Section for Automation and Control, University of Aalborg, Denmark. She has published more than 100 conference and journal papers. In 2006 she received the IEEE Transactions on Control Systems Technology Outstanding Paper Award. She is a senior member of IEEE and Associate Editor of the IEEE Transactions on Control Systems Technology. She furthermore holds several board positions in industrial and research companies. Her research interests include nonlinear control of mechanical systems with applications to robotics, satellites, AUVs and ships.

**Øyvind Stavdahl** (M'09) was born in Lillehammer, Norway, 1967. He received the MSc and PhD from the Department of Engineering Cybernetics, Norwegian University of Science and Technology (NTNU), Trondheim, Norway, in 1994 and 2002, respectively. He became a Research Scientist in 1998 and in 2004 a Senior Scientist at SINTEF ICT, Department of Applied Cybernetics, where he currently is a Scientific Advisor. In 2004 he became a Postdoctoral Fellow, in 2007 Lecturer and in 2008 Associate Professor at the Department of Engineering Cybernetics, NTNU. In 2005 he was a Visiting Fellow at the Institute of Biomedical engineering, University of New Brunswick, Fredericton, NB, Canada. Dr. Stavdahl was a Board Member of the Norwegian Association of Automatic Control 2008-2010. His research interests include rehabilitation engineering, human movement analysis and biomimetic robotics.

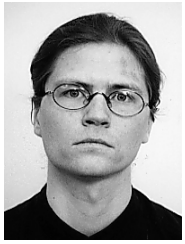

**Tommy Gravdahl** (S'94–M'98–SM'04) graduated siv.ing (1994) and dr.ing (1998) in engineering cybernetics at the Norwegian University of Science and Technology (NTNU), Trondheim, Norway. He was appointed Associate Professor (2001) and Professor (2005) at the Department of Engineering Cybernetics, NTNU. In the academic year 2007/08 he was Visiting Professor with The Centre for Complex Dynamic Systems and Control (CDSC), The University of Newcastle, Australia. He has published more than 75 papers at conferences and in journals and is author of Compressor Surge and Rotating Stall: Modeling and Control (London, Springer, 1999), co-author of Modeling and Simulation for Automatic Control (Trondheim, Marine Cybernetics, 2002) and co-editor of Group Coordination and Cooperative Control (Berlin, Springer, 2006). His current research interests include mathematical modeling and nonlinear control in general, modeling and control of turbomachinery and control of spacecraft, robots and nanopositioning devices. Professor Gravdahl received the IEEE Transactions on Control Systems Technology Outstanding Paper Award in 2000 and is member of the editorial board of Simulation Modeling Practice and Theory.